Energy profiles for light impurities in simple metals

S. Estreicher*
Institut für Theoretische Physik, Universität Zürich, Schönberggasse 9, CH-8001 Zürich, Switzerland

P. F. Meier
Physik-Institut der Universität Zürich, Schönberggasse 9, CH-8001 Zürich, Switzerland
(Received 22 July 1982)

The self-consistent density-functional formalism has been used to calculate electronic densities around light interstitial impurities in jellium. The resulting charge densities have been fitted to a simple analytic expression and the fit parameters determined as functions of r_s for all metallic densities. Energy profiles have then been calculated in 17 simple metals with the use of up to six different local pseudopotentials in first-order perturbation theory. The dependence of the energy on the choice of pseudopotential is discussed. In some cases it was possible to predict the stable interstitial site and the most probable diffusion paths. The zero-point energy of positive muons and protons in the calculated potentials has been estimated and the problem of localization discussed. The effect of the zero-point motion of the lattice ions is shown to be negligible. The modification of the energy profiles with lattice relaxation has been studied in the case of Al.

I. INTRODUCTION

There is an increasing interest in the behavior of hydrogen in metals which is due in part to the technological importance of hydrogen in metallurgy and hydrogen storage materials and in part to the basic solid-state physics problems involved. From the theoretical point of view, the interaction of a single proton with a metallic host is one of the simplest impurity problems, since the proton is a point charge with no complicating core electron structure. However, it is precisely the absence of core electrons which gives rise to a strong electron-proton potential which cannot be treated within a linearized screening approximation.

The behavior of particles with a unit positive charge is also relevant to the positive muon (μ^+) and pion (π^+) which, in recent years, have been used as probes in solids. As concerns the interactions with the ions and electrons in metals, muons and pions behave identically to the proton and its heavier isotopes deuterium and tritium. However, the large mass difference ($m_p \cong 6.7 m_\pi \cong 8.9 m_\mu$) implies very different diffusion properties: The excitation energies for thermally activated diffusion and the tunneling matrix elements, which determine the rate of bandlike diffusion at low temperatures, strongly depend on the particle mass. Further, the amplitude of the zero-point motion and the zero-point energy also change considerably from one particle type to the other, giving rise to a variety of interesting phenomena that can be studied.

A microscopic-theoretical prediction of the diffusion properties requires detailed knowledge of the potential energy of the particle in the host lattice. Various approaches have been developed to calculate potentials for hydrogen in metals. Molecular-cluster and band-structure calculations have been used to investigate particular aspects of the electronic structure of point defects in metals.[1]

Two other approaches have been proposed which simplify the interaction with the lattice ions by introducing pseudopotentials. In the spherical solid model,[2–5] the electron density is calculated in a spherically averaged potential consisting of the bare Coulomb potential of the impurity and the ion pseudopotentials. This method has recently been successfully[6] used to explain Knight shifts at muons at interstitial sites in almost all simple metals. To investigate energy profiles, however, another approach which starts with the jellium model and takes into account the anisotropy of the lattice as a perturbation, seems equally appropriate. We chose this second approach, which was first used for protons in Al and Mg by Popovic and Scott.[7] The metal is first approximated by a homogeneous interacting electron gas with a positive background (consisting of the smeared-out positive ions) of density

$$n_0 = \frac{3}{4\pi} r_s^{-3} . \tag{1}$$

The jellium parameter r_s is thus defined as the radius of the sphere occupied by one electron in the jellium. For metallic densities, its value varies from

1.87 (Be) up to 5.63 (Cs). The impurity is then implanted and the perturbed charge density calculated. Finally, the positive background is replaced by a pseudopotential at each lattice site. In first-order perturbation theory, the energy of a muon or a proton at $\vec{R}_\mu$ is given by the simple expression

$$E(\vec{R}_\mu)=\sum_{\vec{\Gamma}}\left[\frac{Z}{|\vec{R}_\mu-\vec{R}_{\vec{\Gamma}}|}+\int d^3r\,\Delta n(\vec{r}-\vec{R}_\mu)W(\vec{r}-\vec{R}_{\vec{\Gamma}})\right]+E_0\ , \tag{2}$$

where E_0 contains all terms independent of $\vec{R}_\mu$, $\Delta n(\vec{r})=n(\vec{r})-n_0$ is the displaced electron density, and $W(\vec{r})$ is the difference between the local unscreened pseudopotential and the electrostatic potential of the positive background charge of the jellium. Since we do not calculate the total heat of solution but are only interested in energy differences at various sites, we drop all constant terms.

Since the total displaced charge must be equal to one, Eq. (2) can be rewritten as

$$E(\vec{R}_\mu)=\sum_{\vec{\Gamma}}\int d^3r\,\Delta n(\vec{r})\left[\frac{Z}{|\vec{R}_\mu-\vec{R}_{\vec{\Gamma}}|}+W(\vec{r}-\vec{R}_{\vec{\Gamma}}+\vec{R}_\mu)\right]. \tag{3}$$

All pseudopotentials show a long-range behavior $W(r)=-Z/r$ for r exceeding some core radius r_c. Therefore the two terms in the large parentheses of Eq. (3) cancel each other for r values smaller than $|\vec{R}_{\vec{\Gamma}}-\vec{R}_\mu|-r_c$. This implies that the interaction is weak if the screening of the point charge is completed within a short distance. The smallest r value which gives a contribution to the integral in Eq. (3) is the one where the first overlap with the pseudopotential core occurs. It is therefore of crucial importance that the displaced charge density $\Delta n(\vec{r})$ including its long-ranged Friedel oscillations is calculated exactly.

Various authors[2,7,8] have reported calculations of the energy of protons in Al or Mg using this procedure. The results differ not only in the numerical values of the barrier heights but also in the interstitial site of minimum energy. These discrepancies are due to the use of different pseudopotentials, or to differently calculated charge densities.

The present work gives a systematic attempt to cope with these problems. The charge density around a point charge has been calculated in the framework of the self-consistent density-functional formalism for various jellium densities. We gave particular attention to the self-consistency of $\Delta n(r)$, also in the long-range region. These calculations are described in Sec. III. To allow further use of these results for other calculations, we parametrized the obtained $\Delta n(r)$ in terms of a simple analytic function of r and r_s (Sec. III). To get insight into the accuracy of the use of pseudopotentials, we have calculated the energy profiles for 17 simple metals using up to 6 different local pseudopotentials proposed in the literature. These forms, as well as the calculation of the energy, are reported in Sec. IV. As expected, the energies obtained depend on the choice of the pseudopotential. However, in many cases, it is possible to make definite statements about the possibility of localization of muons or protons and to estimate the heights of diffusion barriers. In some cases, the different pseudopotentials lead to quite different energy profiles, since the contributions from the first few shells partially cancel or correspond to r values where Δn is almost zero. In Sec. V we discuss the results for the bcc, fcc, and hcp metals investigated. In Sec. VI, the influence of lattice relaxation of the first two shells around an impurity at the octahedral and the tetrahedral interstitial sites is discussed in the case of Al.

II. CALCULATION OF THE PERTURBED CHARGE DENSITY

Hohenberg, Kohn, and Sham[9–12] have put forward a theory of the ground-state properties of the electron gas in the presence of an external potential $V_{\rm ext}(\vec{r})$. The ground-state energy is written as a functional of the electron density $n(\vec{r})$:

$$E[n(\vec{r})]=\int d^3r'V_{\rm ext}(\vec{r}')n(\vec{r}')+T_0[n(\vec{r})]+\tfrac{1}{2}\int d^3r'\frac{n(\vec{r})n(\vec{r}')}{|\vec{r}-\vec{r}'|}+E_{\rm xc}[n(\vec{r})]\ , \tag{4}$$

where $T_0[n(\vec{r})]$ is the kinetic energy of a system of noninteracting electrons having density $n(\vec{r})$, and $E_{\rm xc}[n(\vec{r})]$ is the exchange-correlation energy functional of the interacting system. The true ground-state density $n(\vec{r})$ minimizes the energy functional $E[n(\vec{r})]$. A variational principle then reduces the N-body problem to a one-body problem within an exact scheme. Thus, one is left with a set of one-body Schrödinger equations with an effective potential

$$\{-\tfrac{1}{2}\Delta+V_{\text{eff}}[\vec{r},n(\vec{r})]\}\psi_i(\vec{r})=\epsilon_i\psi_i(\vec{r}) . \quad (5)$$

Although this point has already been widely discussed earlier (see, e.g., Ref. 13), it should be recalled that the ψ_i's are not electron wave functions, but correspond to "pseudoparticles."

The effective potential is a functional of the charge density $n(\vec{r})$ and consists of three parts: the external potential V_{ext}, the Coulomb-Hartree term, and the exchange-correlation potential V_{xc}:

$$V_{\text{eff}}[n(\vec{r}),\vec{r}]=V_{\text{ext}}(\vec{r})+\int d^3\vec{r}'\frac{n(\vec{r}')}{|\vec{r}-\vec{r}'|}+V_{\text{xc}}[n(\vec{r})] . \quad (6)$$

The relevant quantity of the theory, the charge density, is then given by a sum of individual densities up to the Fermi level:

$$n(\vec{r})=\sum_i |\psi_i(\vec{r})|^2\Theta(\epsilon_F-\epsilon_i) . \quad (7)$$

While the kinetic and electrostatic parts are treated exactly, an approximation must be used for V_{xc}, which is not known. The most commonly used approximation is the so-called local density approximation (LDA).[10] The exchange-correlation energy is approximated by

$$E_{\text{xc}}[n(\vec{r})]\approx\int d\vec{r}\,\epsilon_{\text{xc}}(n(\vec{r}))n(\vec{r})+O(|\vec{\nabla}n(\vec{r})|^2) , \quad (8a)$$

where $\epsilon_{\text{xc}}(n(\vec{r}))$ is the exchange-correlation energy per electron in a homogeneous electron gas of density $n(\vec{r})$, thus

$$V_{\text{xc}}[n(\vec{r})]=\frac{\delta E_{\text{xc}}[n(\vec{r})]}{\delta n(\vec{r})}\approx\epsilon_{\text{xc}}(n(\vec{r}))+\left.\frac{nd\epsilon_{\text{xc}}(n)}{dn}\right|_{n=n(\vec{r})} . \quad (8b)$$

The approximation, being based on an expansion in powers of $|\vec{\nabla}n(\vec{r})|$, therefore assumes that the charge density does not vary too much over distances comparable to r_s. Although this is not the case near the impurity, the approximation remains good since the potential close to the origin is largely dominated by the Coulomb part.

Equations (5)–(7) need to be solved self-consistently to determine the electron density.

In the following, we consider the external potential produced by a positive point charge located at the origin:

$$V_{\text{ext}}(r)=-\frac{1}{r} . \quad (9)$$

The spherical symmetry can then be used to write down the equation for the radial part of the single-particle wave function $U_{kl}(r)=rR_{kl}(r)$:

$$\left[\frac{d^2}{dr^2}-\frac{l(l+1)}{r}-2V_{\text{eff}}(r)+k^2\right]U_{kl}(r)=0 \quad (10)$$

and

$$n(r)=\frac{1}{\pi^2}\int_0^{k_F}dk\sum_l(2l+1)\frac{1}{r}\left|\frac{U_{kl}(r)}{\alpha_l}\right|^2+n_{\text{bs}}(r) , \quad (11)$$

where α_l is a normalization constant. Here n_{bs} denotes the contribution of the bound state which occurs for $r_s\geq 1.9$. The corresponding energies are shown in Fig. 1 as a function of r_s. The bound states are quite shallow close to $r_s=2$ but they still contribute in a non-negligible way to the total charge density. For scattering states, one needs typically 7 or 8 partial waves and about 40 values of k. This implies that the differential equation (10) has to be solved nearly 300 times for each iteration, up to a radius of five or six times r_s, where the potentials can be set equal to zero and the solution matched to that of the free-electron case.

To obtain a self-consistent solution, one iterates the procedure by inserting the charge density $n(r)$ obtained from (7) into the equations determining the effective potential (6). However, the direct iteration does not converge.

The first approximate solution was proposed by Popovic and Stott,[7,14] who used a two-parameter potential $V_{\alpha\beta}$ for V_{eff}:

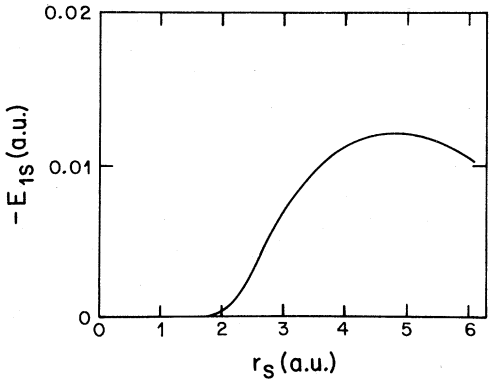

FIG. 1. Energy of the 1s bound state for a point charge ($Z=1$) in jellium vs the parameter r_s.

$$V_{\alpha\beta}=-\frac{e^{-\alpha r^{\beta}}}{r} . \tag{12}$$

The solution was assumed to be self-consistent if α and β were chosen in such a way that the Friedel sum rule was fulfilled with both the trial potential $V_{\alpha\beta}$ and the effective potential V_{eff} constructed after one iteration.

Following Popovic and Stott, we have calculated this two-parameter potential $V_{\alpha\beta}$ for various densities of the electron gas. This solution leads to surprisingly good results for high densities of the electron gas (e.g., in the case of Al or Mg), but fails for higher values of r_s where the absence of iterations using the exchange-correlation potential generates errors which increase with r_s. Further, in the case of low densities of the electron gas, the lack of electrons increases the screening distance and makes of $V_{\alpha\beta}$ too poor an approximation for V_{eff}. As a result, the Friedel oscillations are out of phase and the contact density is overestimated by a large amount. This is illustrated in Fig. 2, where the fully self-consistent result is compared to the approximate solution obtained from the procedure of Popovic and Stott in the extreme case of Cs ($r_s=5.63$). Additionally, it should be mentioned that for low densities of the electron gas it becomes very difficult to find values of α and β which fulfill the requirement of charge conservation with satisfactory precision.

The problem of convergence of the fully self-consistent equations was solved by Manninen *et al.*[15,16] who proposed two tricks which assure the convergence for all metallic densities. First, the determination of the electrostatic part of V_{eff} requires at each iteration (i) the solution of the Poisson equation

$$\Delta V_{\text{es}}^{(i)}(r)=-4\pi n^{(i)}(r) , \tag{13}$$

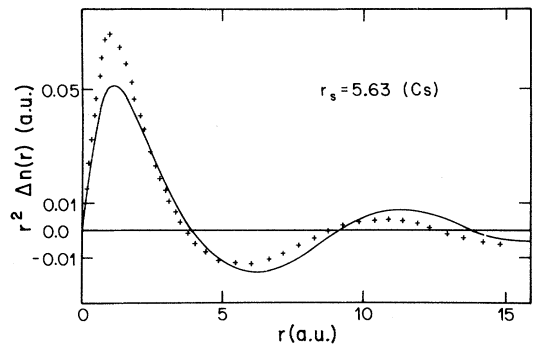

FIG. 2. Comparison between the fully self-consistent charge density (solid line) and the results obtained from the method of Popovic and Stott (Ref. 7, crosses) for low densities of the electron gas. $r_s=5.63$ corresponds to Cs, the metal with lowest electron density.

which leads to the long-ranged integral

$$V_{\text{es}}^{(i)}(r)=\int d^3r' \frac{n^{(i)}(r')}{|\vec{r}-\vec{r}'|} . \tag{14}$$

In Eqs. (13) and (14), $n(r)$ contains all the charge density (impurity, electrons, and background). By subtracting from both sides of (13) the term $q^2V_{\text{es}}^{(i)}(r)$ (where q is a real constant) and replacing on the right-hand side (rhs) $V_{\text{es}}^{(i)}$ by $V_{\text{es}}^{(i-1)}$, Eq. (13) is transformed into a Helmholtz-type equation, the solution to which is nicely convergent:

$$V_{\text{es}}^{(i)}(r)=\int d^3r' \frac{e^{-q|\vec{r}-\vec{r}'|}}{|\vec{r}-\vec{r}'|} \times\left[n^{(i)}(r')-\frac{1}{4\pi}q^2V_{\text{es}}^{(i-1)}(r')\right] . \tag{15}$$

It can be shown[17] that the best choice for q is the Thomas-Fermi screening length

$$q=k_{\text{TF}}=\left[\frac{4k_F}{\pi}\right]^{1/2} . \tag{16}$$

The second trick uses a feedback technique, which prevents too large oscillations of $n^{(i)}(r)$ around the self-consistent solution $n^{\text{sc}}(r)$ from occurring. Instead of writing for iteration (i)

$$V_{\text{eff}}^{(i)}=V_{\text{es}}^{(i)}+V_{\text{xc}}^{(i)} , \tag{17}$$

one uses the effective potential obtained from iteration $(i-1)$ and writes

$$V_{\text{eff}}^{(i)}=\alpha(V_{\text{es}}^{(i)}+V_{\text{xc}}^{(i)})+(1-\alpha)V_{\text{eff}}^{(i-1)} . \tag{18}$$

With a reasonable choice of $\alpha(r_s)$, or even $\alpha(r_s,r)$, the self-consistent procedure converges for all densities of the electron gas.

We used these techniques to calculate the perturbed charge densities for $r_s=2$, 2.2, 2.5, 3, 3.5, 4, 4.5, 5, 5.5, and 6. Equation (10) was solved up to a radius R larger than $6r_s$ using the Numerov method[18] for partial waves up to $l=8$. The density $n(r)$ was calculated using about 50 values of k. The calculations were performed within the local density approximation for V_{xc}, and we used the parametrized form of the result of Singwi *et al.*[19] proposed by Hedin and Lundqvist.[20] Thanks to the computing facilities available, we could iterate the solution a very large number of times (more than one hundred iterations for large r_s values) to make sure that convergence was achieved at every point.

The iteration procedure was started by assuming some screened Coulomb potential as an initial V_{eff}. After a few iterations the values of the charge densi-

ty at the origin as well as of the first maximum of $r^2n(r)$ were already within a few percent of their final values. Further iterations then changed the extrema of the first and second Friedel oscillations, and the self-consistency of $n(r)$ was built up gradually from 0 to larger r values. To achieve convergence also at the extrema of the further oscillations, a large number of iterations was needed for $r_s > 3.5$. This is due to the more pronounced influence of the exchange and correlation potential as compared to the high-density region where the rapidly oscillating densities $n(r)$ could be determined fully self-consistently already after 20 to 30 iteractions. In order to allow easier use for further applications, we found it convenient to parametrize[21] the resulting self-consistent densities, using a simple analytic expression which depends only on r_s.

III. PARAMETRIZATION OF THE SELF-CONSISTENT DENSITY

It is known that the charge density $\Delta n(r) = n(r) - n_0$ fulfills three conditions.

Charge conservation:

$$\int d^3r\, \Delta n(\vec{r}) = 1 . \tag{19}$$

Asymptotic behavior:

$$\Delta n(r \to \infty) = A \frac{\cos(2k_F r + \phi)}{r^3} . \tag{20}$$

Cusp condition:

$$\frac{d}{dr} \Delta n(r) \bigg|_{r=0} = -2\Delta n(0) . \tag{21}$$

The last condition is a direct consequence of the Schrödinger equation (5), and is valid for each individual partial wave if the potential behaves as $-1/r$ close to the origin; this is the case in the local density approximation.

A convenient parametrization of $\Delta n(r)$ can be obtained using the function

$$\Delta n(r) = \frac{1}{\pi} e^{-2r} + \left[\Delta n(0) - \frac{1}{\pi} \right] e^{-2r(1+r)} + f(2k_F r) , \tag{22}$$

which consists of the hydrogen $1s$ charge density, a contribution giving the correct contact density and slope at the origin, and a function f which accounts for the oscillations. Equations (20) and (21) imply that f must be chosen in such a way that $f(0) = f'(0) = 0$ and $f(r \to \infty) = A \cos(2k_F r + \phi)/r^3$. A possible choice for f is a linear combination of Riccati-Bessel functions $\hat{j}_l(x) = x j_l(x)$, where j_l are the usual spherical Bessel functions. We exploited the fact that the zeros of f are strictly linear functions of r_s to parametrize separately the regions $r < Z_2$ and $r > Z_2$, Z_2 being the second zero of f given by

$$Z_2 = 1.52 r_s + 0.462 . \tag{23}$$

The parametrized form was chosen as (with x standing for $2k_F r$):

$$f(x) = \frac{A_0}{x^4+1} \hat{j}_0(x)(1 - e^{-x}) + \frac{1}{x^3+1} \sum_{l=1}^{3} A_l \hat{j}_l(x), \quad r < Z_2 \tag{24}$$

$$f(x) = \frac{1}{x^3+1} \sum_{l=2}^{5} B_l \hat{j}_l(x), \quad r > Z_2 .$$

We are left with a number of parameters which have to be expressed as functions of r_s: the contact density $\Delta n(0)$ and the amplitudes A_l and B_l.

The behavior of the contact density is shown in Fig. 3. Since one expects that for large values of r_s the contact density approaches that of hydrogen, it is natural to parametrize $\Delta n(0)$ by a function that tends asymptotically to $1/\pi$. An inspection of a log-log plot of $\Delta n(0) - 1/\pi$ vs r_s indicates that a very good parametrization in the range $2 \le r_s \le 6$ is given by

$$\Delta n(0) = \frac{1}{\pi} + \exp(-0.72 - 1.28 \ln r_s - 0.385 \ln^2 r_s) . \tag{25}$$

The amplitudes A_l and B_l are smooth functions of r_s (see Ref. 21). Their values, in the range $2 \le r_s \le 6$, have been fitted to a power series in $1/r_s$, which is given in Table I.

The precision of the fit is illustrated in Fig. 4

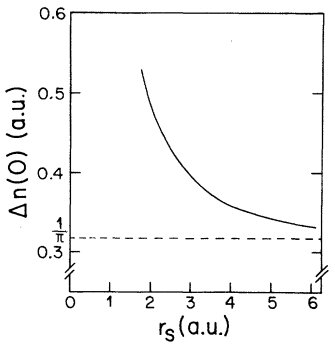

FIG. 3. Contact density $\Delta n(0) = n(0) - n_0$ at the impurity vs the jellium parameter r_s.

TABLE I. Amplitudes of the parametric form for the perturbed charge density as functions of r_s.

l	a_l	b_l	c_l	d_l	e_l
		(a) $r<Z_2$: $A_l=a_l/r_s^4+b_l/r_s^3+c_l/r_s^2+d_l/r_s+e_l$			
0	−9.879	10.795	−4.422	0.696	−0.018
1	0.347	2.257	−1.711	0.927	−0.103
2	14.900	−20.780	10.200	−2.769	0.233
3	−15.040	17.681	−8.380	1.946	−0.156
		(b) $r>Z_2$: $B_l=a_l/r_s^4+b_l/r_s^3+c_l/r_s^2+d_l/r_s+e_l$			
2	−6.197	5.882	−1.256	−0.379	0.047
3	−4.056	6.326	−6.186	1.631	−0.120
4	2.388	−6.313	6.083	−1.688	0.122
5	−16.430	19.463	−9.391	1.820	−0.114

which shows the self-consistent curve and the parametrized function on the same graph in the case of Au ($r_s=3$). The electron densities obtained from the parametrized form have been compared to the results of other authors[17,22,23] and good agreement has always been found. Excellent agreement exists also between the Fourier transform of the calculated $\Delta n(r)$ and that of the parametrized expression. Furthermore, the total displaced charge Eq. (19) calculated with the values from Table I was found to be very close to 1 for all values of r_s from 1.8 to 6.0. We also investigated the effect on the charge density of the choice of the parametrized form for the exchange-correlation potential V_{xc}. We repeated the calculations using the Wigner formula[24] for V_{xc} at $r_s=4$ and found a small difference in the amplitude of the first two oscillations of $r^2\,\Delta n(r)$. This difference was in all cases larger than that existing between the self-consistent result and the parametrized form.

IV. CALCULATION OF THE ENERGY AND PSEUDOPOTENTIALS

A. Theoretical formulation

Equation (2) can be written as the sum of two terms.

(a) The first term, depending only on the lattice structure, is evaluated using Ewald's method for lattice sums:

$$E_{\rm str}(\vec{R}_\mu)=Z\left[\sum_{\vec{l}}\frac{1}{|\vec{R}_\mu-\vec{R}_{\vec{l}}|}\,\mathrm{erfc}(G\,|\vec{R}_\mu-\vec{R}_{\vec{l}}\,|)+\frac{4\pi}{\Omega_0}\sum_{\vec{g}}{}'\frac{\cos\vec{g}\cdot\vec{R}_\mu}{g^2}e^{-g^2/4G^2}-\frac{\pi}{\Omega_0 G^2}\right]=\frac{Za_B}{a}X(\vec{R}_\mu)\,. \tag{26}$$

The constant G can be chosen in such a way that both sums converge rapidly. $\vec{g}$ is a reciprocal-lattice vector, a the lattice constant, and Ω_0 the atomic volume. $X(\vec{R}_\mu)$ is related to the Madelung energy $M(\vec{R}_\mu)$ defined as[2]

$$E_{\rm str}(\vec{R}_\mu)=\frac{Z^{2/3}}{r_s}M(\vec{R}_\mu)\,. \tag{27}$$

Since $a=r_s Z^{2/3}(3/4\pi n)^{-1/3}$ ($n=2$ for bcc, $n=4$ for fcc), $X(\vec{R}_\mu)$ and $M(\vec{R}_\mu)$ differ only by a constant. $X(\vec{R}_\mu)$ is plotted in Fig. 5 for $\vec{R}_\mu$ moving on a straight line from the octahedral (O) to the tetrahedral (T) sites for bcc, fcc, and hcp lattices. It can be seen that the emptiest lattice (bcc) is the one where $E_{\rm str}$ is the smallest.

Another feature should be mentioned: We have

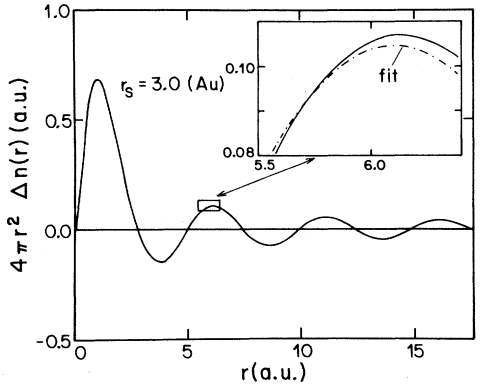

FIG. 4. Plots of the fully self-consistent charge density around a positive muon or a proton in jellium with $r_s=3.0$ (Au) and of the density obtained from the parametrized form [Eqs. (22)–(25)]. Both curves can be distinguished in the inset.

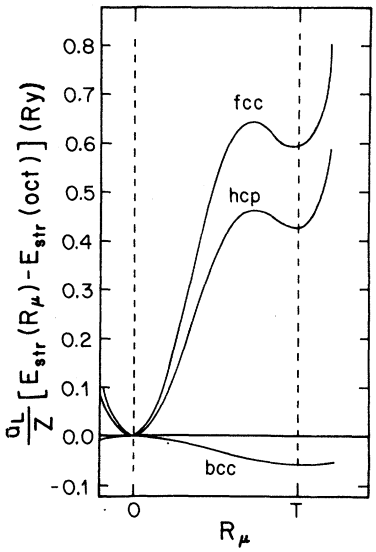

FIG. 5. The part of the energy which depends only on the structure [Eq. (26)] for bcc, fcc, and hcp (ideal c/a) lattices.

calculated[25] the volume of a sphere that fits into the space left at various sites by touching spheres centered on the lattice points. In the fcc lattice, the volume V_{oct} at the octahedral site is 6.2 times larger than the volume V_{tet} at the tetrahedral site. In the hcp case (with ideal c/a ratio), $V_{oct}=6.3V_{tet}$. But in the bcc lattice, $V_{oct}=(1/6.7)V_{tet}$. It follows from these simple considerations that the structural part of the energy is always a minimum where the maximum space is available.

(b) The second term of Eq. (2), which also depends on the structure, contains all interactions between electrons. We therefore called it the interaction part of the energy:

$$E_{int}(\vec{R}_\mu)=Z\frac{1}{\Omega_0}\sum_{\vec{g}}{}'\cos(\vec{g}\cdot\vec{R}_\mu)\Delta n(g)W(g)\ . \tag{28}$$

$\Delta n(g)$ and $W(g)$ are the Fourier transforms at reciprocal-lattice vectors of the perturbed charge density and of the pseudopotential. As has been mentioned in the introduction, E_{int} largely compensates E_{str} if the impurity is screened over distances short compared to the nearest-neighbor distance.

This is the case in metals with small r_s values, which happen to crystallize in the fcc or hcp structure. On the other hand, in metals with low density of the electron gas (large r_s values), which are the bcc metals, the main part of the energy is given by E_{str}. Examples will be mentioned in Sec. V.

B. Pseudopotentials

As mentioned in Sec. I the different values published for the energies of protons or muons in Al suggest that in addition to the exact form of the perturbed electron density $\Delta n(r)$, the choice of the pseudopotential could be crucially important. In the latter case one has to regard all results for the energy profiles with great caution since it is possible that the description of the electron-core interaction by a local pseudopotential is too crude to reliably predict the interaction energies of point charges. In order to obtain a general feeling, we investigated the results obtained from six different local pseudopotentials commonly used in the literature. Five of them are one- or two-parameter potentials obtained either from the Ashcroft empty-core pseudopotential or from the simplified Heine-Abarenkov pseudopotential. They differ by an exponential screening in $\vec{q}$ space, as q^n. We denote therefore the pseudopotentials with an upper index n. In Fourier space, these pseudopotentials are

$$W_A^0(q)=\frac{-4\pi}{q^2}Z\cos qr_c\ , \tag{29}$$

which is the bare Ashcroft empty-core pseudopotential, with a screened form

$$W_A^2(q)=\frac{-4\pi}{q^2}Z\cos qr_c e^{-(q/5.5k_F)^2}\ . \tag{30}$$

The bare simplified Heine-Abarenkov pseudopotential is

$$W_{HA}^0=\frac{-4\pi}{q^2}Z\left[\lambda\frac{\sin qr_c}{qr_c}+(1-\lambda)\cos qr_c\right]\ , \tag{31}$$

with the two screened forms

$$W_{HA}^2(q)=\frac{-4\pi}{q^2}Z\left[\lambda\frac{\sin qr_c}{qr_c}+(1-\lambda)\cos qr_c\right]\times e^{-(q/5.5k_F)^2} \tag{32}$$

and

$$W_{HA}^4(q)=\frac{-4\pi}{q^2}Z\left[\lambda\frac{\sin qr_c}{qr_c}+(1-\lambda)\cos qr_c\right]\times e^{-\xi(k/2k_F)^4} \tag{33}$$

with $\xi=0.03$ for alkali metals and 0.15 for Al. Finally, a pseudopotential was computed by Borchi and De Gennaro[26,27] for noble metals using four parameters:

$$W^0_{\mathrm{BG}}(q)=\frac{-4\pi}{q^2}Z\left[\cos qr_2+\frac{\lambda}{q}(\sin qr_2-\sin qr_1-qr_2\cos qr_2+qr_1\cos qr_1)-\frac{V_0}{q}(\sin qr_1-qr_1\cos qr_1)\right]. \quad (34)$$

r_1 has been set equal to 1 a.u. for Cu, Ag, and Au, and r_2 chosen in such a way that $r_1+r_2=r_i$, the Pauling ionic radius.

The parameters r_c and λ can be calculated from a large number of experimental properties of the pure solid (transport properties, phonon spectrum, bulk modulus, lattice constant, . . .). Fixing the parameters for one given pseudopotential to different properties of the metal leads of course to different numbers for these parameters. A complete list of experimental properties used by various authors would be too long: The parameters used in our calculations as well as the references to the authors who determined them for bcc, fcc, and hcp simple metals, respectively, are given in Sec. V. The interest of the screening in $\vec{q}$ space lies in the fact that all sums over reciprocal lattice vectors converge nicely. However, it should be noticed that in direct space this corresponds to making the pseudopotential a continuous function with continuous derivatives. This can be seen in Fig. 6 where $W^0_A(r)$, $W^2_A(r)$, $W^0_{\mathrm{HA}}(r)$, and $W^2_{\mathrm{HA}}(r)$ are plotted in $\vec{r}$ space in the case of Al.

V. RESULTS

A. bcc metals

The bcc lattice with all possible symmetric interstitial sites is shown in Fig. 7; the hexagons denote the octahedral sites (O), the triangles the tetrahedral sites (T), and the small circles some of the triangular sites (Tr).

The sites of interest for an interstitial impurity are along the following directions: from the T site,

(1) $\langle 100\rangle$: T-O-T, with distance $d=\frac{1}{2}a$ between the two T sites

(2) $\langle 110\rangle$: T-Tr-T, $d=\frac{\sqrt{2}}{4}a$,

(3) $\langle 111\rangle$: T-T, $d=\frac{\sqrt{3}}{2}a$,

and from the O site,

(1) $\langle 110\rangle$: O-O, $d=\frac{\sqrt{2}}{2}a$,

(2) $\langle 111\rangle$: O-O, $d=\frac{\sqrt{3}}{2}a$.

We have calculated the potentials along all of these directions using the available pseudopotentials (see Table II) for all alkali metals and for Ba.

As an example, Fig. 8 shows the energy profiles in the case of K. Only the curves corresponding to the pseudopotentials predicting the lowest and highest barriers are indicated. The dotted line shows the structural part of the energy [Eq. (26)].

The potentials look very similar for all alkali met-

TABLE II. Pseudopotential parameters for the simple metals crystallizing in the bcc structure with references to the authors who determined them. The table also contains the value of the jellium parameter r_s, the valence Z, and the lattice constant a. All quantities are in atomic units.

Element	Z	W^0_A (Refs. 28–35)		W^2_A (Refs. 4 and 5)	W^0_{HA} (Refs. 7, 36, and 42)		W^2_{HA} (Ref. 4)		W^4_{HA} (Refs. 39–41)	
r_s	a	r_c		r_c	r_c	λ	r_c	λ	r_c	λ
Li	1	1.038	1.06	1.29	1.559	0.408	1.26	−0.070	1.512	0.334
3.253	6.592	1.40	1.678		1.562	0.373	1.32	0.081	1.531	0.367
									1.534	0.371
Na	1	1.61	1.663	1.53	2.081	0.308	1.50	−0.075	2.071	0.363
3.941	7.984	1.69	1.758		2.173	0.480	1.56	0.063	2.116	0.422
K	1	2.047	2.107	2.10	3.016	0.572	2.30	0.300	2.972	0.540
4.834	9.874	2.135	2.226		3.099	0.624			3.010	0.570
Rb	1	2.02	2.125		3.486	0.697			3.384	0.640
5.187	10.554	2.256	2.40		3.545	0.727			3.360	0.631
Cs	1	2.104	2.16		3.997	0.768			3.795	0.680
5.628	11.423	2.425	2.62		4.114	0.808			3.863	0.709
		2.93								
Ba	2	2.55								
3.698	9.496									

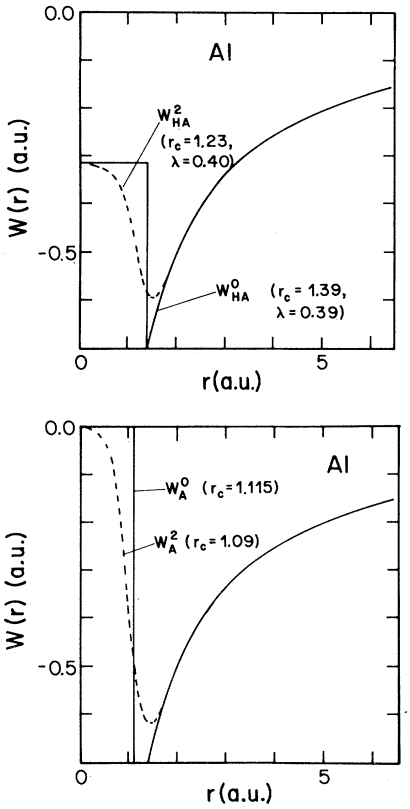

FIG. 6. Comparison between the behaviors of various pseudopotentials in $\vec{r}$ space. The introduction of screening in $\vec{q}$ space modifies the hard-core picture and makes the pseudopotential a continuous function with continuous derivative.

als: The same site (T) corresponds to a minimum of the energy. The heights of the barriers are of the same order of magnitude for all elements from Li down to Cs. It should be noted that the lowest barriers always coincide with the bare Ashcroft pseudo-

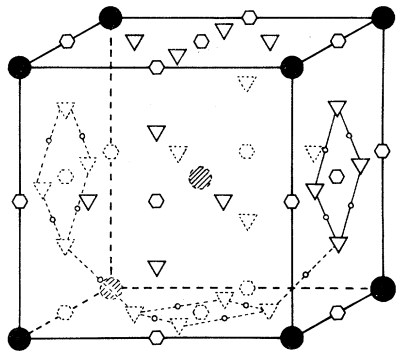

FIG. 7. bcc lattice with all octahedral (hexagons), all tetrahedral (triangles), and some triangular sites (small circles).

potential W^0_A, while the highest barriers correspond to the most screened pseudopotential (W^4_{HA}). However, for Ba with $Z=2$ (where the only pseudopotential published is W^0_A) the barriers are much larger than those in alkali metals.

The small heights of the barriers between T sites which are of the order of 0.1—0.2 eV raise the question whether light impurities can be localized at all. The exact calculation of the zero-point motion of muons or protons requires a detailed consideration of the impurity wave function in the real three-dimensional anharmonic potential. This point will be discussed elsewhere.

In order to get a rough estimate of the zero-point energy E_0 of a muon or a proton, we have approximated the potentials by a parabola going through the minimum and the inflection point, and have determined E_0 in the harmonic potential $V(r)=\rho r^2$, which is

$$E_0=\frac{3}{2}\left[\frac{2\rho}{m}\right]^{1/2} . \tag{35}$$

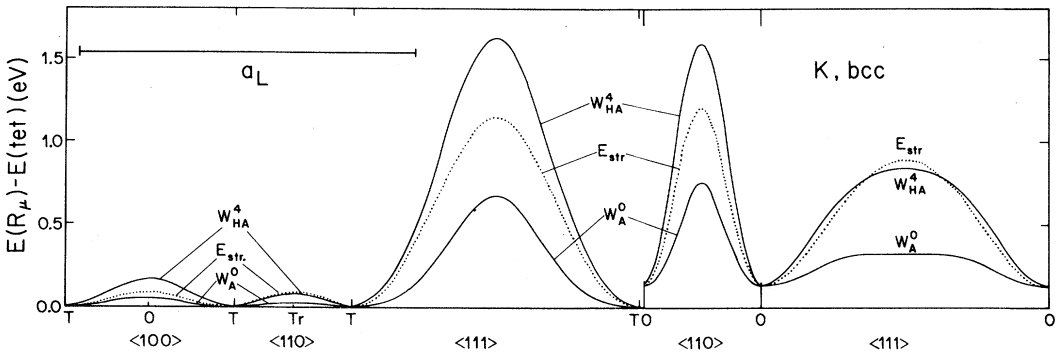

FIG. 8. Energy profiles calculated for an impurity in K along a straight line in different directions from a T site or an O site. Only the curves corresponding to pseudopotentials predicting the highest and the lowest barriers are plotted (solid lines): the upper curve always corresponds to W^4_{HA} and the lower to W^0_A. The dotted line shows the structural part of the energy E_{str}, and a_L the lattice constant.

TABLE III. Minimal (H_{min}) and maximal (H_{max}) heights of the barriers predicted by various pseudopotentials between equivalent adjacent sites in the bcc lattice along various directions (see Fig. 8) in K, which is a representative of alkali metals, and Ba. An estimate of the zero-point energy of a muon and a proton is given in each case. All energies are in eV.

		K					Ba		
Direction	H_{min}	$E_0(\mu^+)$	$E_0(p^+)$	H_{max}	$E_0(\mu^+)$	$E_0(p^+)$	H	$E_0(\mu^+)$	$E_0(p^+)$
T-O-T, ⟨100⟩	0.045	0.06	0.02	0.160	0.14	0.05	0.296	0.13	0.04
T-Tr-*T*, ⟨110⟩	0.016	0.09	0.03	0.070	0.18	0.06	0.116	0.145	0.05
T-T, ⟨111⟩	0.672	0.15	0.05	1.630	0.28	0.09	3.262	0.17	0.06
O-O, ⟨110⟩	0.627	0.35	0.12	1.468	0.21	0.07	2.966	0.26	0.09
O-O, ⟨111⟩	0.195	0.13	0.05	0.713	0.25	0.08	1.083	0.19	0.06

where $m=m_\mu$ or m_p is the mass of the impurity in a.u. and ρ the curvature of the parabola. This rough estimate makes sense when the obtained values of E_0 are either much smaller or much larger than the height H of the barrier, indicating the existence or nonexistence of an obstacle for diffusion.

Table III gives the height H and the values of $E_0(\mu)$ and $E_0(p)$ in the cases of K (representative of alkali metals) and Ba. This table indicates that a proton could be trapped at the T site in Ba, but not in any alkali metal at least when effects of lattice relaxation are neglected (see Sec. VI). On the other hand, a muon cannot be localized in any of these bcc metals.

Another rough estimate has been made to account for the effect of lattice vibrations at $T=0$ K. The Fourier transform of the second term in the rhs of Eq. (2) is

$$\sum_{\vec{l}}\int d^3r\,\Delta n(\vec{r}-\vec{R}_\mu)W(\vec{r}-\vec{R}_{\vec{l}})=\frac{1}{(2\pi)^3}\int d^3q\,e^{i\vec{q}\cdot\vec{R}_\mu}\Delta n(q)W(q)\sum_{\vec{l}}e^{-i\vec{q}\cdot\vec{R}_{\vec{l}}(t)}\,, \tag{36}$$

TABLE IV. Pseudopotential parameters for the simple metals crystallizing in the fcc structure with references to the authors who determined them. The table also contains the value of the jellium parameter r_s, the valence Z, and the lattice constant a. All quantities are in atomic units.

		W_A^0 (Refs. 28, 29, 31	W_A^2 (Refs. 4	W_{HA}^0 (Refs. 7, 37,	W_{HA}^2 (Ref. 5)		W_{HA}^4 (Ref. 41)		W_{BG}^0, $r_1=1$ (Refs. 26 and 27)		
Element	Z	32, and 34)	and 5)	38, and 42)							
r_s	a	r_c	r_c	r_c	r_c	λ	r_c	λ	r_2	λ	V_0
Cu	1	0.813		2.42	1.125				1.815	0.50	1.90
2.664	6.831										
Ag	1	1.039		2.73	1.160				2.38	0.68	2.95
3.023	7.721										
Au	1	0.813		2.72	1.398				2.60	0.50	2.66
3.005	7.708										
Ca	2	1.905									
3.269	10.548										
Sr	2	2.13									
3.554	11.499										
Al	3	1.115	1.09	1.388	0.397	1.23	0.398	1.247	0.350		
2.072	7.653	1.131		1.394	0.389			1.247	0.361		
				2.20	1.188			1.269	0.332		
				2.20	1.159			1.273	0.542		
								2.457	1.211		
Pb	4	1.077		2.40	1.020						
2.304	9.356	1.12									
		1.474									

where

$$\vec{R}_\Gamma(t)=\vec{R}^0_\Gamma+\vec{u}_\Gamma(t)\ , \tag{37}$$

with

$$\langle u_\Gamma(t)\rangle=0\ . \tag{38}$$

Since we are interested only in an order of magnitude of the effect of $\vec{u}_\Gamma(t)$, we used the Debye-Waller approximation for the time-dependent exponential

$$\langle e^{-i\vec{q}\cdot\vec{u}(t)}\rangle=e^{-q^2\langle u^2\rangle/6}\ . \tag{39}$$

Thus, the net effect of zero-point lattice vibration is to screen the pseudopotential by the factor $e^{-q^2\langle u^2\rangle/6}$. In the Debye approximation, for $T=0$ K and in atomic units,

$$\langle u^2\rangle=\frac{64.546}{A\Theta_D}\ , \tag{40}$$

where A is the atomic number of the ion and Θ_D is the Debye temperature. The product $A\Theta_D$ being always large, we are left with small numbers for $\langle u^2\rangle$ ($0.14a_B^2$ for Li, $0.07a_B^2$ for Cs) and the effect of this additional screening is small. As a result, the potential barriers are lowered or raised by amounts which are never larger than 0.007 eV. Numbers of this order of magnitude are much smaller than the barriers themselves and out of proportion with the precision expected from calculations in first-order perturbation theory. We therefore neglected this contribution in the following.

B. fcc metals

The fcc lattice and all octahedral and tetrahedral sites are shown in Fig. 9. The sites of interest are along the following directions:

(1) $\langle 100\rangle$: T-T, with distance $d=\frac{1}{2}a$ between two adjacent T sites .

(2) $\langle 111\rangle$: T-O-T, along the body diagonal of the cube, both T sites being at the distance $(\sqrt{3}/2)a$.

(3) $\langle 110\rangle$: O-O, with $d=(\sqrt{2}/2)a$.

We calculated the energy profiles along these directions for all pseudopotentials (see Table IV).

Figure 10 shows the profiles obtained in the case of Al in these directions. For the $\langle 100\rangle$ and $\langle 110\rangle$ directions, we represented only the highest and lowest barriers as well as the structural part of the energy $E_{\rm str}$ (dotted line). Along the $\langle 111\rangle$ direction the results corresponding to various choices for the pseudopotential differ from each other and five typical curves are represented. The results for this T-O-T barrier obtained by other authors are also shown and fit rather well with our own calculations.

The problem of deciding whether a proton prefers to sit at the O or T site in Al can obviously not to be solved with the present model, since the results depend too strongly on the pseudopotential. However, it seems probable that a muon will not see a significant potential barrier in the $\langle 111\rangle$ direction from the T to O site, no matter what pseudopotential is used to determine its diffusion properties.

In contrast to the bcc case, the structural part of the energy always differs from $E(\vec{R}_\mu)$ by a large amount. As mentioned in Sec. I, this is related to the small r_s values characterizing fcc (and hcp) metals. It should also be noticed that the highest barriers coincide with $W^0_{\rm HA}$ and not with the most screened pseudopotential $W^4_{\rm HA}$, as in the bcc case. However, the smallest barriers are still those calcu-

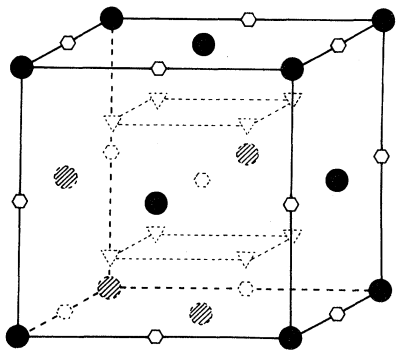

FIG. 9. fcc lattice containing octahedral (hexagons) and tetrahedral (triangles) sites.

TABLE V. Height H of the potential barriers along the $\langle 100\rangle$ (T-T) and the $\langle 111\rangle$ (T-O-T) directions in Sr and Ca. The zero-point energies of a muon and a proton are indicated. Both a μ^+ and a p^+ seem to be strongly localized at the T site. All energies are in eV.

	Direction	H	$E_0(\mu^+)$	$E_0(p^+)$
Sr	$\langle 100\rangle$, T-T	0.84	0.34	0.11
	$\langle 111\rangle$, T-O-T	1.17	0.24	0.08
Ca	$\langle 100\rangle$, T-T	0.93	0.37	0.12
	$\langle 111\rangle$, T-O-T	1.02	0.24	0.08

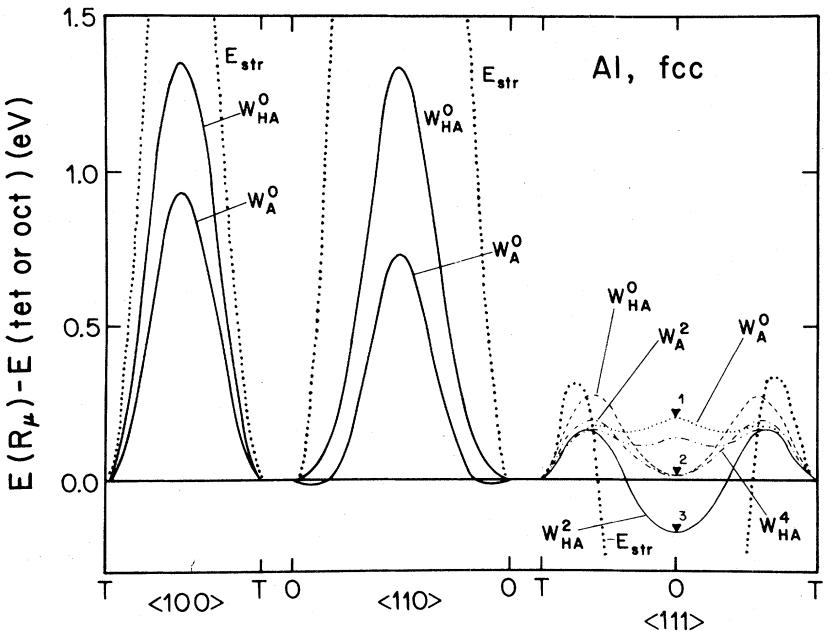

FIG. 10. Potentials seen by an impurity along various directions in Al. Along the ⟨100⟩ and ⟨110⟩ directions, only the curves corresponding to pseudopotentials predicting the highest and lowest barriers are plotted. In the case of the ⟨111⟩ direction, five curves are shown, and the triangles indicate the results obtained by other authors: Larsen and Norskov (1), Ref. 8, Manninen and Nieminen (2), Ref. 2, and Popovic and Stott (3), Ref. 7.

lated with W_A^0.

The situation in other fcc metals differs from one element to the other.

(a) In Pb, all three pseudopotentials lead to very different results as concerns the site of lowest energy. However, the barrier heights are always quite small in at least one of the three directions: W_A^0 (with $r_c=1.474$) gives the lowest barrier along the ⟨100⟩ direction, W_A^0 with $r_c=1.077$ along the ⟨110⟩ direction, and W_{HA}^0 along the ⟨111⟩ direction. Thus, neither a proton nor a muon is expected to be localized.

(b) The situation is different in Ca and Sr. The bare Ashcroft pseudopotential (which in all previous cases predicted the lowest barriers when compared to other pseudopotentials) predicts a strong localization of both muons and protons at the T site (see Table V).

(c) The potentials along all directions are shown in Fig. 11 for the noble metals, using the bare simplified Heine-Abarenkov pseudopotential which is called the "Nikulin pseudopotential" by some authors.

In the ⟨100⟩ direction (T-T), the height of the po-

TABLE VI. Pseudopotential parameters for the simple metals crystallizing in the hcp structure with references to the authors who determined them. The table also contains the value of the jellium parameter r_s, the valence Z, and the lattice constant a. All quantities are in atomic units.

Element	Z		W_A^0 (Refs. 28, 29, and 32)	W_{HA}^0 (Ref. 7)	
r_s	a	c/a	r_c	r_c	λ
Be	2		1.055		
1.874	4.318	1.567			
Mg	2		1.358	1.69	0.451
2.642	6.064	1.624	1.39		
Zn	2		1.11		
2.304	5.025	1.856	1.272		
Cd	2		1.247		
2.590	5.629	1.886			

tential barrier decreases rapidly as one goes from Cu to Au. This is even more pronounced along the ⟨110⟩ direction (*O-O*). The difference is still more marked along the ⟨111⟩ direction: in Cu, the *O*-site has lowest energy (E_0-E_T = −0.6 eV, Teichler[43,44] predicted some −0.8 eV) where a proton and even a muon could be localized. In Ag, the proton could still be localized at the *O* site, whereas more detailed calculations are needed in order to determine whether a muon could be localized or not. In Au, the minimum in the *T-O-T* direction corresponds to the *T* site with E_0-E_T=0.48 eV. Therefore, in Au, the lowest barrier is along the ⟨100⟩ direction between two *T* sites. The potential of Borchi and Gennaro W^0_{BG} also predicts a strong localization of muons and protons at the *O*-sites in Cu (with E_0-E_T = −1.6 eV), much less localized in Ag (E_0-E_T = −0.3 eV) and again strongly localized in Au (E_0-E_T = −0.85 eV). These results are in contradiction with those obtained from the bare Ashcroft pseudopotential W^0_A which gives in general much smaller barriers and wells, preventing any localization.

C. hcp metals

The hcp structure with the *O* and *T* sites is shown in Fig. 12. The *O* sites lie in the $Z=\frac{1}{4}c$ and $Z=\frac{3}{4}c$ planes, while the *T* sites lie in slightly displaced planes. This is due to the presence of an ion nearby in the $Z=\frac{1}{2}c$ plane. Thus, in the *c* direction the sequence for symmetric sites is the following: *O-O-O* ⋯ or *T*-ion-*T*-*T*-ion-*T* ⋯ .

The sites of interest lie along the following directions:

(1) ⟨001⟩: *O-O*, with distance $d=\frac{1}{2}c$ between two neighboring *O* sites .

(2) ⟨110⟩: *O-O*, with $d=a$, in the $Z=\frac{1}{4}c$ plane .

(3) ⟨10∼0⟩: *O-T*, with $d_{OT}=\frac{1}{3}[3+a^2/c^2]^{1/2}a$ when going from an *O* site to the nearest *T* site .

(4) ⟨001⟩: *T* with $d=\left[\frac{1}{2}\frac{c}{a}-\frac{2}{3}\frac{a}{c}\right]a$.

In the ⟨110⟩ direction joining two *T* sites lying in the same plane ($d=a$) a high barrier always exists ($2.3<H<4.9$ eV) for all elements and all pseudopotentials (see Table VI).

The energy profiles in Mg are shown in Fig. 13 for two pseudopotentials. The structural part of the energy (dotted line) differs, as for fcc metals, by an order of magnitude from the full energy $E(\vec{R}_\mu)$. The results published by Popovic *et al.*[14] are represented by triangles. The curves indicate a slight minimum at the *T* sites, which is too shallow to localize a muon or even a proton.

In Zn, the barriers are quite high between *O* sites (0.8 eV for *O-O* in the ⟨001⟩ direction and 1.11 eV for *O-O* in the ⟨110⟩ direction) as well as between *T* sites along the ⟨001⟩ direction (0.42 eV). The lowest barrier corresponds to the *O-T* jump (0.36 eV) with a slight minimum at the *T* site ($E_0-E_T\simeq-0.1$ eV). Because of the very short distances between nearest *O* and *T* sites this is not sufficient to localize a μ^+.

For Ca, all barriers are extremely flat. As in the cases of Mg and Zn, the tetrahedral site has lowest energy (E_0-E_T=0.36 eV).

The situation is different in the case of Be, where all barriers are very high and where the *T* site has a much larger energy than the *O* site (E_T-E_0=0.7 eV). The heights of the barriers as well as zero-point energies of muons and protons are given in Table VII. It seems that protons and muons are strongly localized at *O* sites in Be. There is some experimental evidence for muons being localized in Be.[45]

VI. EFFECT OF LATTICE RELAXATION

We have calculated the effect of lattice expansion or contraction of the first two shells in the case of Al. We supposed that the lattice ions are displaced around a given interstitial site $\vec{R}_s=\vec{R}_{oct}$ or $\vec{R}_{tet}$ in the radial direction:

$$(\vec{R}_s-\vec{R}_\gamma)\rightarrow(1+\delta_i)(\vec{R}_s-\vec{R}_\gamma)\ , \tag{41}$$

TABLE VII. Height *H* of the potential barriers along the ⟨001⟩, ⟨110⟩, and ⟨10∼0⟩ directions in Be and estimates of the zero-point energies of muons and protons in these potentials. Both particles might well be localized at the *O* site in Be.

Direction		*H*	$E_0(\mu^+)$	$E_0(p^+)$
⟨001⟩,	*O-O*	1.27	0.70	0.24
⟨110⟩,	*O-O*	3.25	0.80	0.27
⟨10∼0⟩,	*O-T*	1.18	0.73	0.24

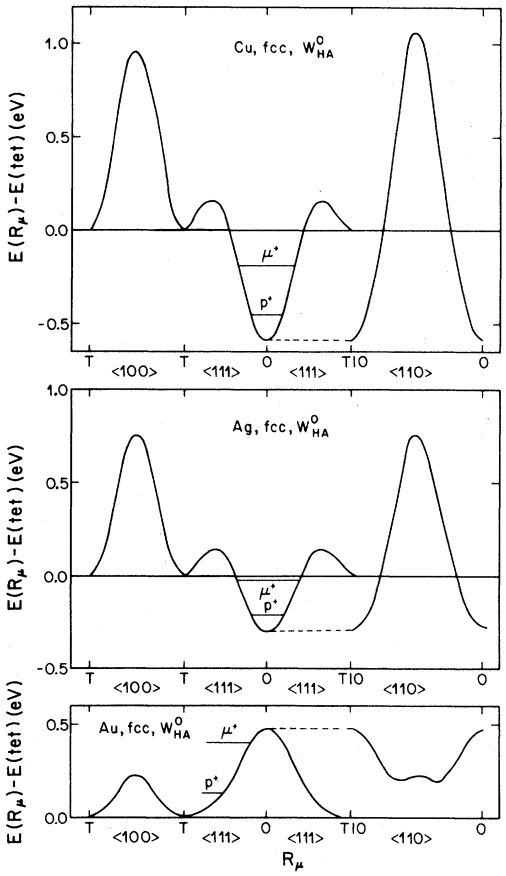

FIG. 11. Energy profiles in noble metals obtained with W^0_{HA}. The zero-point energies of a proton and a muon are indicated. The potentials are similar to those predicted by the four-parameter potential W^0_{BG} (see Table IV) in the case of Cu and Ag, but not in Au where W^0_{BG} predicts a deep well (−0.85 eV) at the O site.

where i numbers the shells. We fixed the displacement of the second shell to be

$$\delta_2=\pm\tfrac{1}{5}\delta_1 \ . \tag{42}$$

If $E^0(\vec{R}_\mu)$ stands for the unperturbed energy and

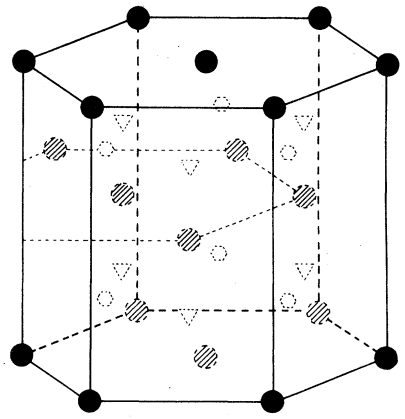

FIG. 12. hcp lattice with its octahedral (hexagons) and tetrahedral (triangles) sites.

$E^{\rm rel}(\vec{R}_\mu)$ for the relaxed one, the change in the energy is

$$E^{\rm rel}(\vec{R}_\mu)-E^0(\vec{R}_\mu)=\sum_{\vec{l}}[E(X^{\rm rel}_{\vec{l}})-E(X^0_{\vec{l}})] \ , \tag{43}$$

where the sum goes over the ions $\vec{l}$ which are relaxed, and where

$$X^0_{\vec{l}}=|\vec{R}_\mu-\vec{R}_{\vec{l}}| \tag{44}$$

and

$$X^{\rm rel}_{\vec{l}}=|\vec{R}_\mu-\vec{R}_{\vec{l}}+\delta_i(\vec{R}_s-\vec{R}_{\vec{l}})| \ . \tag{45}$$

The function $E(X)$ has been calculated in the Appendix [see (A11)].

The resulting change in energy is shown in Fig. 14 for $\vec{R}_s=\vec{R}_{\rm oct}$ and $\delta_2=+0.2\delta_1$. δ_1 was varied from −0.06 to 0.06, and its value is indicated on each curve. The curves in Fig. 14 have been calculated using the bare Ashcroft pseudopotential W^0_A with $r_c=1.115$. An expansion of the first shell together with an expansion of the second shell lowers the energy at the T site, but does not significantly perturb the energy at the neighboring O site. We have also

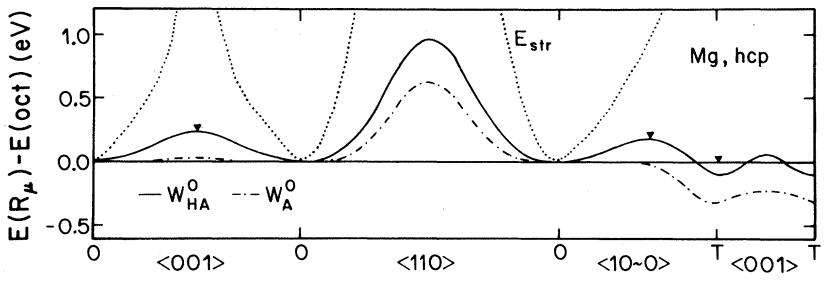

FIG. 13. Potentials obtained with W^0_A (dashed line) and W^0_{HA} (full line) in Mg along various directions. The triangles show the results calculated by Popovic and Stott (Ref. 7) using W^0_{HA}.

calculated the effect of lattice relaxation for $\vec{R}_s = \vec{R}_{oct}$ and found that even a large expansion or contraction about the O site does not render it more stable.

It should be mentioned that the influence of the second shell is rather small in Al as has been checked by changing the sign of δ_1/δ_2 in both cases.

Perrot and Rasolt[5] have calculated anisotropic lattice relaxation effects for a proton in Al, using W_A^2 and W_{HA}^2. They found a relaxation energy of -0.06 eV corresponding to $\delta_1 = 2$–$3\,\%$ in magnitude.

As can be seen from Eq. (2), the change in energy upon relaxation will depend on the sign and magnitude of $\Delta n(r)$ at the first few neighboring shells. A more detailed study will be published elsewhere.

VII. SUMMARY AND CONCLUSIONS

With the use of the self-consistent density-functional method, the electron density around a unit positive point charge in jellium has been calculated and parametrized for $2.0 < r_s < 6.0$. These results have then been used to compute energy profiles in 17 simple metals using many different pseudopotentials in first-order perturbation theory. The dependence of the energies on the choice of the pseudopotential, which in some cases is strong, exhibits the relative weakness of this approach. Nevertheless, a good physical insight can be gained on the behavior of hydrogenlike impurities in most simple metals. The heights of potential barriers can often be estimated within some 20%. Additionally, the sites of lowest energy and the easiest diffusion paths can be predicted in many cases. The question whether the impurity can be localized or not has been investigated.

Hydrogen-diffusion experiments[46] show a much smaller activation energy in bcc metals than in hcp and fcc lattices. We observed the same trends in our calculations. In alkali metals with the bcc structure, the barriers along the ⟨100⟩ (T-O-T) as well as along the ⟨110⟩ (T-Tr-T) directions never exceed 0.2 eV, favoring an easy diffusion of light impurities. In bcc Ba, only a proton or one of its heavier isotopes could be localized at the T site.

The situation is different in fcc and hcp simple metals: In Al and Pb, muons and protons see almost no barrier along the body diagonal of the cube (⟨111⟩, T-O-T direction). However, a strong localization at the T site is predicted for both Ca and Sr. In Cu, two pseudopotentials predict a localization of muons and protons at the O site, and all our calculations indicate a much weaker localization in Ag. For Au, the results obtained using different pseudopotentials are in contradiction. Muon spin resonance experiments[47] in Cu show a localization of muons below 100 K at the octahedral site. Blocking experiments on the localization of pions[48] in Au are in preparation. The muon diffusion rate at high temperatures[49] decreases when going from Au to Ag and to Cu.

In hcp Mg, Zn, and Cd no high barriers are present, whereas light interstitials may easily be trapped at the O sites in Be.

Since a small lattice relaxation ($<3\%$ in magnitude), does not too strongly affect these results, a more detailed study seems necessary only in the cases where the zero-point energy of the impurity is of the same order of magnitude as the barrier heights. A full treatment of lattice relaxation and of the zero-point motion (including a calculation of the

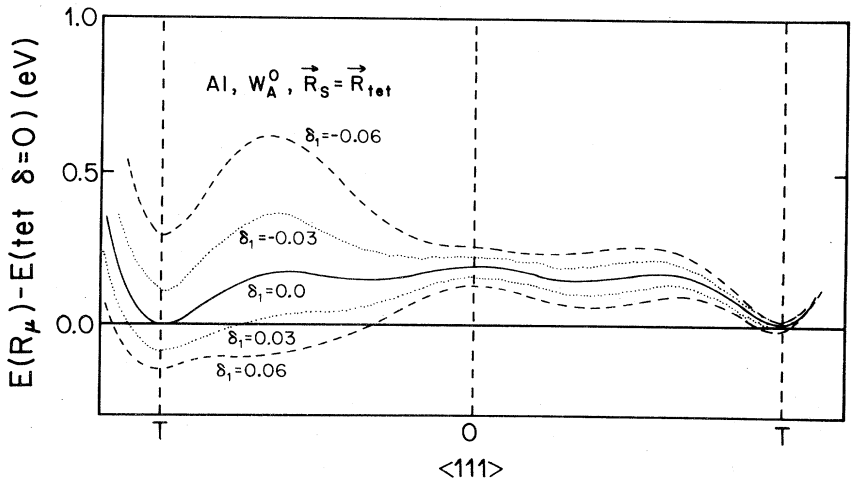

FIG. 14. Effect on the energy profile along the ⟨111⟩ direction in Al when the lattice is relaxed about one of the T sites. The first shell is relaxed in the radial direction by $\delta_1 = -6\%$ up to $\delta_1 = +6\%$, and the second shell by $\delta_2 = +0.2\delta_1$. The value of δ_1 is indicated on each curve. The full line corresponds to the rigid lattice.

impurity wave function in the anharmonic three-dimensional potential) is then needed to give reliable results. This is the case in Au, Al, and Zn. More details about these effects will be published elswhere.

ACKNOWLEDGMENTS

The authors would like to express their gratitude to M. Manninen for numerous instructive discussions and suggestions and to A. B. Denison and B. D. Patterson for critical reading of the manuscript. This work was partially supported by the Swiss National Science Foundation.

APPENDIX: EVALUATION OF THE ENERGY FOR A SINGLE ION

For a single ion at $\vec{R}$, the energy [Eq. (2)] is given by

$$E(\vec{R}_\mu)=\frac{Z}{|\vec{R}-\vec{R}_\mu|}+\int d^3r\,\Delta n(\vec{r}-\vec{R}_\mu)W(\vec{r}-\vec{R})\,. \quad \text{(A1)}$$

With $\vec{X}=\vec{R}-\vec{R}_\mu$ and since $\int d^3r\,\Delta n(\vec{r})=1$, (A1) reduces to

$$E(\vec{X})=\int d^3s\,\Delta n(\vec{s})\left[\frac{Z}{X}+W(\vec{s}-\vec{X})\right]. \quad \text{(A2)}$$

In the case of the Ashcroft empty-core pseudopotential:

$$W(\vec{s}-\vec{X})=-\frac{Z}{|\vec{s}-\vec{X}|}+\frac{Z}{|\vec{s}-\vec{X}|}\Theta(r_c-|\vec{s}-\vec{X}|)\,, \quad \text{(A3)}$$

one can split (A2) into two parts:

$$E(\vec{X})=Z\int d^3s\,\Delta n(\vec{s})\left[\frac{1}{X}-\frac{1}{|\vec{s}-\vec{X}|}\right]+Z\int d^3s\,\Delta n(\vec{s})\frac{1}{|\vec{s}-\vec{X}|} \quad \text{(A4)}$$

$$=E_\infty(\vec{X})+E_{\text{core}}(\vec{X})\,. \quad \text{(A5)}$$

With the use of the expansion of $1/|\vec{s}-\vec{X}|$ into Legendre polynomial and the orthonormality relation of the P_l's, E_∞ is easily reduced to

$$E_\infty(X)=\frac{Z}{X}4\pi\int_X^\infty dr\,\Delta n(r)(r-X)=\frac{Z}{X}[F(X)-XG(X)]\,, \quad \text{(A6)}$$

where

$$F(X)=4\pi\int_X^\infty dr\,r^2\Delta n(r)$$

and

$$G(X)=4\pi\int_X^\infty dr\,r\Delta n(r)\,. \quad \text{(A7)}$$

It is also easy to write $E_{\text{core}}(\vec{X})$ as a linear combination of the functions F and G: If one renames $\vec{t}=\vec{s}-\vec{X}$ and takes the Fourier transform of $\Delta n(\vec{t}+\vec{X})$, the integral over $\vec{t}$ can be calculated with the result

$$E_{\text{core}}(X)=\frac{Z}{X}\frac{2}{\pi}\int_0^\infty dq\,\Delta n(q)\frac{\sin qX(1-\cos qr_c)}{q}\,. \quad \text{(A8)}$$

One returns to $\vec{r}$ space by taking the inverse Fourier transform of $\Delta n(q)$, and calculating the integral over q,

$$E_{\text{core}}(X)=\frac{Z}{X}4\pi\left[\int_0^X dr\,r^2\Delta n(r)+X\int_0^\infty dr\,r\Delta n(r)-\tfrac{1}{2}\int_0^{X+r_c}dr\,r^2\Delta n(r)-\tfrac{1}{2}(X+r_c)\int_{X+r_c}^\infty dr\,r\Delta n(r)-\tfrac{1}{2}\int_0^{X-r_c}dr\,r^2\Delta n(r)-(X-r_c)\int_{X+r_c}^\infty dr\,r\Delta nr\right]. \quad \text{(A9)}$$

Since

$$\int_0^X dr\,r^2\Delta n(r)=F(0)-F(X)\,, \quad \text{(A10)}$$

the sum $E_\infty(X)+E_{\text{core}}(X)$ can be done and one obtains

$$E(X)=\frac{Z}{2X}[F(X+r_c)+F(X-r_c)-X(G(X+r_c)+G(X-r_c))-r_c(G(X+r_c)-G(X-r_c))]\,. \quad \text{(A11)}$$

*Present address: Physics Department, Rice University, P.O. Box 1892, Houston, TX 77251.

[1]P. Jena, in *Treatise on Materials Science and Technology* (Academic, New York, 1981), Vol. 21, p. 351.

[2]M. Manninen and R. M. Nieminen, J. Phys. F 9, 1333 (1979).

[3]L. M. Kahn, F. Perrot, and M. Rasolt, Phys. Rev. B 21, 5594 (1980).

[4]F. Perrot, Phys. Rev. B 16, 4335 (1977).

[5]F. Perrot and M. Rasolt, Solid State Commun. 36, 579 (1980).

[6]M. Manninen (unpublished).

[7]Z. D. Popovic and M. J. Stott, Phys. Rev. Lett. 33, 1164 (1974).

[8]D. S. Larsen and J. K. Norskov, J. Phys. F 9, 1975 (1979).

[9]P. Hohenberg and W. Kohn, Phys. Rev. B136, 864 (1964).

[10]W. Kohn and L. J. Sham, Phys. Rev. A 6, 1967 (1965).

[11]W. Kohn and L. J. Sham, Phys. Rev. 140A, 1133 (1965).

[12]L. J. Sham and W. Kohn, Phys. Rev. 145, 561 (1966).

[13]V. L. Moruzzi, J. F. Janak, and A. R. Williams, *Calculated Properties of Metals* (Pergamon, New York, 1980).

[14]Z. D. Popovic, M. J. Stott, J. P. Carbotte, and G. R. Piercy, Phys. Rev. B 13, 590 (1976).

[15]M. Manninen, R. M. Nieminen, P. Hautojarvi, and J. Arponen, Phys. Rev. B 12, 4012 (1975).

[16]R. M. Nieminen, J. Phys. F 7, 375 (1977).

[17]M. Manninen, private communication.

[18]G. W. Pratt, Phys. Rev. 88, 1217 (1952).

[19]K. S. Singwi, A. Sjölander, M. P. Tosi, and R. H. Land, Phys. Rev. B 1, 1044 (1970).

[20]L. Hedin and B. I. Lundqvist, J. Phys. C 4, 2064 (1971).

[21]S. Estreicher and P. F. Meier, Nato Series on Materials Science (in press).

[22]K. Petzinger, private communication.

[23]P. Jena, Hyperfine Interact. 6, 5 (1979); A. K. Gupta, P. Jena, and K. S. Singwi, Phys. Rev. B 18, 2712 (1978).

[24]E. Wigner, Phys. Rev. 46, 1002 (1934).

[25]S. Estreicher and P. F. Meier, Phys. Rev. B 25, 297 (1982).

[26]E. Borchi and S. De Gennaro, Phys. Lett. 32A, 301 (1970).

[27]E. Borchi and S. De Gennaro, Phys. Rev. B 5, 4761 (1972).

[28]N. W. Ashcroft and D. C. Langreth, Phys. Rev. 155, 682 (1967).

[29]N. W. Ashcroft and D. C. Langreth, Phys. Rev. 159, 500 (1967).

[30]N. W. Ashcroft, J. Phys. C 2, 232 (1968).

[31]N. W. Ashcroft, Phys. Lett. 23, 48 (1968).

[32]W. M. Shyu and G. D. Gaspari, Phys. Rev. 170, 687 (1968).

[33]D. L. Price, K. S. Singwi, and M. P. Tosi, Phys. Rev. B 2, 2983 (1970).

[34]S. P. Singh, Phys. Rev. B 9, 3313 (1974).

[35]G. Solt and A. P. Zhernov, Solid State Commun. 23, 759 (1977).

[36]P. S. Ho, Phys. Rev. B 3, 4035 (1971).

[37]T. Suzuki, Phys. Rev. B 3, 4007 (1971).

[38]A. I. Gubanov and V. K. Nikulin, Fiz. Tverd. Tela (Leningrad) 7, 2701 (1965) [Sov. Phys.—Solid State 7, 2184 (1966)].

[39]G. Solt and A. P. Zhernov, J. Phys. F 9, 1013 (1979).

[40]A. P. Zhernov and G. Solt, Fiz. Tverd. Tela (Leningrad) 21, 3048 (1979) [Sov. Phys.—Solid State 21, 1754 (1979)].

[41]G. Solt and K. Werner, Phys. Rev. B 24, 817 (1981).

[42]Z. D. Popovic, J. P. Carbotte, and G. R. Piercy, J. Phys. F 4, 351 (1974).

[43]H. Teichler, Hyperfine Interact. 6, 251 (1976).

[44]H. Teichler, Phys. Lett. 67A, 313 (1978).

[45]H. Metz, H. Orth, G. zu Putlitz, A. Seeger, H. Teichler, J. Vetter, W. Wahl, M. Wigand, K. Dorenburg, M. Gladish, and D. Herlach, Hyperfine Interact. 6, 271 (1979).

[46]J. Völkl and G. Alefeld, in *Hydrogen in Metals,* edited by G. A. Alefeld and J. Völkl (Springer, Berlin, 1978), Vol. 1, pp. 321–348.

[47]M. Camani, F. N. Gygax, W. Rüegg, A. Schenck, and H. Schilling, Phys. Rev. Lett. 39, 836 (1977).

[48]K. Maier, private communication.

[49]R. H. Heffner, Hyperfine Interact. 8, 655 (1981).